Pergamon

Cement and Concrete Research 29 (1999) 1441–1453

CEMENT AND CONCRETE RESEARCH

Water retention and granular rheological behavior of fresh C_3S paste as a function of concentration☆

S. Mansoutre[a,b], P. Colombet[a,*], H. Van Damme[b]

[a]*Laboratoire Matériaux, Adjuvants et Technologies, CTG Italcementi Group, Les Technodes B.P. 01, 78931 Guerville, France*
[b]*Centre de Recherches la Matière Divisée, CNRS and Université d'Orléans, 45071 Orléans Cedex 2, France*

Received 27 August 1998; accepted 28 May 1999

Abstract

Water retention and rheological behavior of fresh C_3S paste have been analysed as a function of C_3S volume fraction. Three investigation techniques have been used : (1) the test of water demand, (2) filtration under gas pressure, and (3) shear rheology with normal stress measurements. Cross correlations between shear rheological parameters, dilatancy, and water retention measurement results allow for the construction of a concentration-rheology "phase diagram," ranging from the concentrated suspension regime, where rheology is dominated by hydrodynamic interactions and follows Krieger-Dougherty equation, to the granular paste regime, where rheology is dominated by fluctuations of solid contacts and where dilatancy sets in. © 1999 Elsevier Science Ltd. All rights reserved.

Keywords: Cement paste; C_3S; Rheology; Stability

1. Introduction

New applications for Portland cement pastes, such as super workable concrete (SWC), self-levelling concrete (SLC), ultra-high performance, or concrete for extrusion, require better and better monitoring control of their rheological properties and of solid/liquid segregation phenomena. The general trend is toward the formulation of very concentrated (yet very fluid) pastes, with a very low yield stress. This is achieved by controlling the chemical composition of the cement paste (especially with regard to the aluminate and sulfate contents of the cement), the granular distribution of the mortar or the concrete, and, finally, the interparticular interactions by adsorption of superplasticizers. Simultaneously, homogeneity has to be maintained by avoiding various solid/liquid segregation phenomena such as sedimentation and bleeding (with SWC and SLC) or internal filtration (during extrusion). An integrated picture relating (even qualitatively) rheology and water retention would therefore be very useful. This is the aim of the present paper.

1.1. Suspensions vs. granular media

The rheology and stability of very concentrated pastes, in a regime where the volume of liquid is about what is necessary to fill the void space of the granular packing, can be approached either by using concepts developed for suspension rheology extrapolated at the maximum packing fraction or by using those of granular matter (soil) physics and mechanics. As far as the concentrated suspension approach is concerned, shear flow is by far the most extensively studied deformation mode. In such flows, it is now well established [1] that in spite of their chemical complexity cement slurries follow the classical Krieger-Dougherty equation [2] for viscosity of a dispersed suspension, as seen in Eq. (1):

$$\eta_r = \eta/\eta_c = \left(1 - \frac{\phi_s}{\phi_M}\right)^{-[\eta]\phi_m} \quad (1)$$

where η_r is the relative viscosity, η is the apparent shear viscosity of the suspension, η_c is the apparent shear viscosity of the liquid phase, ϕ_s is the volume fraction of solids, $[\eta]$ is the intrinsic viscosity of the particles, and ϕ_M is the maximum packing volume fraction of solids, which depends on particle size distribution and shape. Eq. (1) was first proposed empirically by Krieger and Dougherty [2] and later derived by Krieger [3], using the concept of "crowding" introduced by Mooney [4] in order to take into account the fact that introducing additional particles in a suspension has a larger energy dissipation effect than introducing them in

☆ This paper was originally submitted to *Advanced Cement Based Materials*. It was received at the Editorial Office of *Cement and Concrete Research* on 27 August 1998 and accepted in final form on 28 May 1999.

* Corresponding author. Tel.: +33-1-34-77-75-82; fax: +33-1-34-77-77-80.

E-mail address: mta@ctg.fr (P. Colombet)

0008-8846/99/$ – see front matter © 1999 Elsevier Science Ltd. All rights reserved.
PII: S0008-8846(99)00129-5

the pure liquid dispersion medium. The cumulative effect of this crowding leads to Eq. (1). In fact, Eq. (1) is the most general among a series of equations of the same general form, $\eta_r = (1 - \phi_s/\phi_M)^{-q}$ that all predict divergence of viscosity as the solid volume fraction approaches the maximum packing fraction ϕ_M [3,5–8]. It fits remarkably well a large number of rheological data obtained on a wide variety of colloidal suspensions [9]. Provided segregation can be avoided, it applies also to suspensions of noncolloidal particles, including Portland cement particles, either well dispersed (with superplasticizer) or flocculated (without superplasticizer) [1]. In the latter case, the solid volume fraction to consider is an effective (envelope) volume fraction of the flocs.

In quasistatic (lower shear rate) conditions with model colloidal systems of hard spheres, ϕ_M is close to the random close packing fraction, 0.63, and [η] is close to the expected value from Einstein theory for dilute suspensions, [η] = 2.5 [10,11]. At a higher shear rate, some ordering of the particles occurs and ϕ_M may approach the value for face centered cubic packing, 0.74.

Of particular interest for the advanced applications mentioned above is what happens as ϕ_s approaches ϕ_M closely (i.e., when crowding becomes dominant). For colloidal hard sphere particles at low shear rate, viscosity tends to infinity, which is equivalent to the onset of a yield stress, τ_y [11]. This yield stress is not related to the formation of any network of aggregated particles. It is simply due to the dense packing of the particles, with flow occurring when the structure is distorted enough to allow particles to move. Interestingly, even in this regime no normal stress is detected [11]. With charged colloidal particles, the same scheme is valid but the densely packed objects to be considered are not the real physical particles but the soft virtual "particles" made of the real particles surrounded by their Debye sphere [12]. The onset of the yield stress is then equivalent to the transition from a sol to a repulsive gel or glass.

Fundamentally different from this is the flow behavior close to ϕ_M of dense packings of noncolloidal particles such as sand, first studied by Reynolds [13] and later by Bagnold [14]. Although the viscous interaction with the pore fluid may still be important, direct interparticular contact is now the dominant phenomenon. This, together with the absence of spontaneous Brownian motion, is at the origin of a number of unusual effects [15]. Among those is the so-called "dilatancy" effect (which should not be confused with shear thickening): the particles are so close to each other that they have to push their neighbours to initiate their motion [14,15]. Thus, beyond a definite density threshold, the packing cannot be sheared any longer without volume expansion. The densely packed material volume must extend in order to make space for grains to pass between each other [13]. The onset of dilatancy corresponds to the minimum packing density that requires expansion to allow internal shear. For monodisperse spherical particles in the zero gravitational acceleration limit (grains and liquid with the same density), this occurs at $\phi_s = 0.56$ [15].

On the other hand, during contact the main dissipation mechanism may be either momentum transfer due to collision or intergrain friction, collision in the rapid flow regime, and friction in the slow deformation rate regime. Since the friction forces between the grains increase as the normal force between those grains increases according to Coulomb's law for friction, shear flow becomes more difficult as a pressure P is applied to the packing. The critical shear stress allowing the onset of flow increases with P according to Eq. (2):

$$\tau_y = \tau_{y0} + \mu P \tag{2}$$

where μ is the coefficient of friction between the grains [16]. In some loading modes, for instance pressure compaction of cement slurries, this may lead to blockage of compaction and to the persistence of internal pores [17].

Another characteristic feature of granular packings under stress is the extremely broad distribution of intergrain contacts [18–20]. Under a given macroscopic load, a large fraction of the contacts do not carry any stress, whereas others transmit most of the load. Furthermore, the pattern of contacts in a given packing is not an equilibrium property but depends on the way the packing was prepared. In other words, it is history dependent. This may lead to strong fluctuations in results (e.g., with regards to measurements).

Adsorption of a polymer or polyelectrolytes on the surface of grains may have two different effects, depending on particle concentration. In the suspension regime, it may deflocculate the suspension due to repulsive interactions, and hence decrease the effective solid volume fraction. In the granular regime, it may lubricate intergrain contacts (i.e., lead to vanishing μ in the second equation). In both cases the ratio of shear stress over shear rate (i.e., the apparent viscosity) is expected to decrease. In this work we shall restrict our concern to the analysis of polymer- and polyelectrolyte-free slurries and pastes, to focus on the consequences of both crowding and intergrain contacts on the rheological behavior.

1.2. Water retention and the thermodynamic state of water

The ability of a well-dispersed suspension, flocculated slurry, or granular packing to retain water under a given stress is a function of the water chemical potential in the system. As a stress is applied, the system loses water until the chemical potential of the residual water, μ_w, equals that imposed by the stress. The stress may be applied in several ways, for instance by equilibrating the paste with a low partial water vapor pressure (i.e., drying the paste) [21] or, alternatively, by applying a pressure on the paste over a porous membrane (i.e., filtering the paste) [22]. Another way of stressing the medium is by equilibrating it with a solution of polymer through a semipermeable membrane (i.e., osmotic stressing) [23]. As long as the system is stable and the transformation is thermodynamically reversible, all ways of applying the stress are equivalent [24].

The residual water content e is a function of the stress intensity or, equivalently, of the imposed chemical potential μ_w [see Eq. (3)].

$$e = f(\mu_W) \tag{3}$$

This function is a powerful way of studying the interactions and the structure of the system (just as a flow curve is in rheology). The water content e may be expressed as the liquid/solid mass ratio, $e = m_w/m_s$, and the chemical potential is related to the activity of water a_w as shown in Eq. (4):

$$\mu_w = \mu_0 + \mathrm{RT\ Ln}\ a_w \tag{4}$$

where μ_0 is as usual the chemical potential of pure water in equilibrium with its saturating vapor pressure (P_0). At equilibrium, the chemical potential (hence the activity) of the liquid water is the same everywhere in the sample, whatever the local concentration of ions, and is equal to the chemical potential μ_v of the vapor surrounding the sample at pressure P_v, as in Eq. (5):

$$\mu_w = \mu_v = \mu_0 + \mathrm{RT\ Ln}\ P_v/P_0 \tag{5}$$

A suspension where $a_w = 1$ would be an infinitely diluted paste, in ions and particles, with $P_v = P_0$.

In a water-saturated paste, the total differential of μ_w may be written as seen in Eq. (6) [24]

$$d\mu_w = -\bar{s}dT + v_w dP_w + \left(\frac{\partial \mu_w}{\partial e}\right)_{T,P,P_g} de + v_w d\Pi \tag{6}$$

where $\bar{s}$ is the partial molar entropy of water, P_w is the pressure in the liquid water, v_w is the molar volume of water, and Π is the solute contribution to osmotic pressure. The term in de is the so-called matrix potential term.

Let us consider a filtration device in which filtration is driven by applying a gas pressure P_g on the suspension above a filter. Provided the interstitial liquid of the suspension is Newtonian, this gas pressure is transmitted to the liquid. On the other hand, the pressure at the bottom of the filter is the atmospheric pressure (P_a). Furthermore, provided the filter remains liquid-saturated, the ionic composition in the filter pores is the same as in the suspension and there is no osmotic pressure difference due to the solute between the suspension and the filtrate. The only osmotic pressure difference is due to the particles in the suspension. In these conditions and in isothermal conditions, Eq. (6) becomes Eq. (7):

$$d\mu_w = v_w dP_w + \left(\frac{\partial \mu_w}{\partial e}\right)_{T,P} de \tag{7}$$

Integration of the above equation from P_a to P_g leads to Eq. (8):

$$\mu_w(P_g, e) - \mu_w^0(P_a, e = \infty) = v_w(P_g - P_a) + \int_\infty^e \frac{\partial \mu_w}{\partial e} de \tag{8}$$

where $\mu_w(P_g,e)$ is the chemical potential of water in the suspension, at a pressure P_g, and where $\mu_w{}^0$ $(P_a,e = \infty)$ is the chemical potential of the particle-free filtrate ($e = \infty$), at the same solute concentration as in the suspension. At equilibrium, both are equal. Since the mass of solid is constant, De = de and Eq. (8) is reduced to Eq. (9)

$$\mu_w - \mu_{ws} = + v_w(P_g - P_a) \tag{9}$$

where μ_{ws} is the chemical potential of water in the filter and the drain. As long as the particles are well separated from each other, the pressure on the dispersion can alternatively be applied using a piston since the pressure is transmitted uniformly throughout the fluid. However, as soon as the particles come into contact, this equivalence is no longer true since part of the forces are transmitted through the solid skeleton.

In the first method of imposing the water chemical potential (drying under reduced water vapor pressure) Eq. (4) and Eq. (5) apply straightforwardly, yielding Eq. (10):

$$\mu_w - \mu_0 = \mathrm{RT\ Ln}\ (P_v/P_0) \tag{10}$$

This method can hardly be applied to liquid dispersions since the relative water vapor pressure (P_v/P_0) in equilibrium with a suspension is very close to 1, making accurate control virtually impossible.

In the dispersed state, when the individual particles or flocs are well separated from each other, the ability of the system to retain water depends on the repulsive forces between the suspended objects and ions. When the particles come into contact and form a connected but porous solid network, the pressure that prevents the water from escaping the network is the so-called capillary pressure, which stems from the meniscus curvature at the water-gas interface. The radius of the menisci in equilibrium with a given water vapor pressure is given by the Kelvin relation [25] shown in Eq. (11):

$$r_k = -2v_w\gamma_{LV}/(\mathrm{RT\ Ln}\ a_w) \tag{11}$$

where γ_{LV} is the liquid/vapor interface tension of water (0.073 Jm^{-2} at room temperature). On the other hand, the pressure difference between the gas phase and the liquid phase is given by the Young-Laplace equation, relating this pressure jump through the interface to the curvature of that interface [25], as can be seen from Eq. (12):

$$P_g - P_a = 2\gamma_{LV}/r_k \tag{12}$$

When taken together, Eqs. (4) through (12) provide a powerful way to derive information about the dispersion structure and its evolution, from the $e = f(\mu_w)$ or $e = f(a_w)$ curve.

In this work, we have used filtration under gas pressure. The general scheme for the structural evolution is as follows (Fig. 1). Starting from a dispersed suspension of C_3S particles (which may be individual grains or small flocs), the first regime of water loss may be an extremely rapid loss under the sole action of gravity if the suspension contains an excess of water with respect to the amount at which no sedimentation nor bleeding would occur. This regime (if any) is followed by one in which progressive water loss is determined at each value of the applied pressure by the equilibrium between the resulting stress and the repulsive forces between particles. As far as rheological measurements are concerned, this is a state where the Krieger-Dougherty equation is expected to be valid.

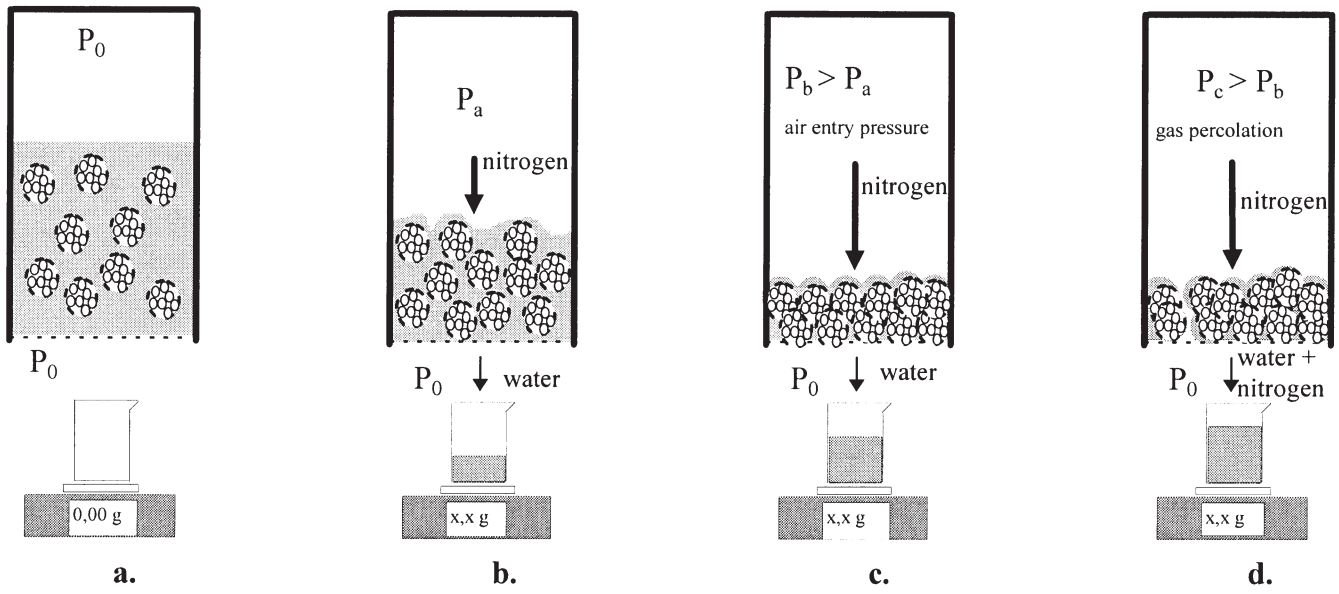

Fig. 1. Schematic structural evolution during filtration under gas pressure. Before applying the gas pressure, the system is in the suspension state and the meniscus is flat (a). Under low pressure (b), the meniscus radius decreases which involves the shrinkage of the system combined with a loss of water. As soon as the compaction of the system is complete, gas begins to enter the porosity of the granular packing; this is the so-called point of air entry (c). At some higher pressure, a continuous path for the gas phase develops within the packing; this is the point of gas phase percolation (d).

A critical point is when the particles come into contact as a consequence of partial water loss and form a porous packing saturated with liquid water. In rheology, this is the regime where a granular-type behavior is expected. Increasing the gas pressure further will first compact the packing, provided the friction forces between particles are not too high [26]. Classical shear rheology may become difficult to carry out at this stage. Above some pressure threshold, the packing becomes too rigid and no longer consolidates. At this stage, increasing the gas pressure compels the menisci, which in previous stages were at the boundary of the paste, to penetrate into the voids of the packing. This is the point of air entry. The system becomes unsaturated. As the pressure is increased further, the gas phase reaches smaller pores according to Eq. (12) and penetrates deeper and deeper into the packing. Finally, at some higher pressure a continuous path for the gas phase develops within the packing. This is the point of gas phase percolation. As far as rheological measurements are concerned, this unsaturated regime is the domain of soil mechanics.

At each state along this process, a given value of the applied gas pressure corresponds to a given value of the water chemical potential, activity, and vapor pressure, and to a given meniscus radius. As long as the system is in the suspension state, these menisci correspond in fact to an average distance between particles [Figs. 1(a) and (b)]. As soon as the system turns into a granular packing, the meniscus radius corresponds to a true meniscus within a porous medium [Figs. 1(c) and (d)]. As suggested above and shown below, water loss (and water demand) measurements and rheology provide very complementary information on the structure of and interactions within a cement paste.

2. Materials and methods

2.1. Synthesis and reactivity

Pure synthetic C_3S was prepared by successive heatings of a mixture of finely divided silica (Aerosil 380 from Degussa, Courbevoie, France) and calcium carbonate (from Prolabo, Fontenay sous Bois, France). The final heating was at 1550°C for 2 h. Powder X-ray diffraction showed C_3S to exhibit the expected triclinic crystal structure (T1). The amount of residual CaO was determined by selective dissolution and was about 1.7 wt%. C_3S was then milled in a tungsten-carbide mill bowl (Sodemi, Sodemi Muizon, France). The mean grain size of ground powder was 8.5 μm and the Blaine specific surface area 4040 cm^2/g. For each sample, 10 g of ground C_3S were mixed with the weight of deionized water corresponding to the desired water:solid ratio using a Vane stirrer. Each paste was first mixed at low speed for 10 s, then at medium speed for 10 s, again at low speed for 10 s, and medium speed for 10 s. Mixing was finished using low speed for 10 s.

The solid volume fraction is given by Eq. (13):

$$\phi_s = \frac{1}{1 + \frac{\rho_s}{\rho_w} \times \frac{w}{s}} \tag{13}$$

where ρ_s is the density of the solid (3.138 g/cm^3 for C_3S) and ρ_w is the density of water and w/s the initial water:solid mass ratio.

The water reactivity of C_3S was determined by the conduction calorimetry method [27] (Fig. 2). Five periods of reaction may classically be identified by following the rate of heat liberation: (1) the initial period; (2) the so-called induc-

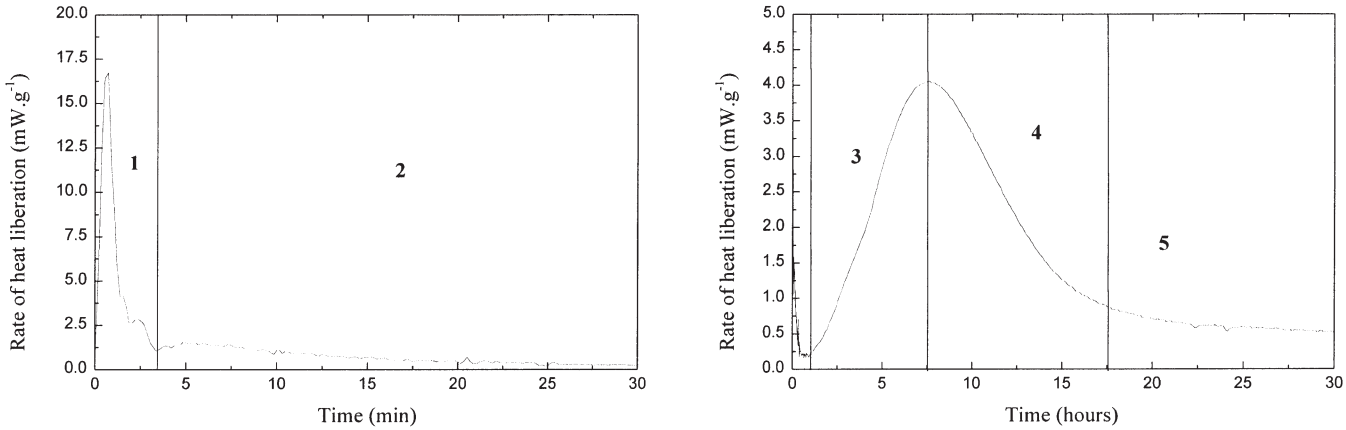

Fig. 2. Rate of heat evolution of the C_3S used in this work, at w/s = 0.50. The five periods of reaction are clearly visible: (1) the initial period, (2) the induction period, (3) the acceleratory period, (4) the deceleratory period, and (5) a period of slow, continued reaction.

tion period (or dormant period); (3) the acceleratory period, in which the main reaction first begins to occur rapidly; (4) the deceleratory period; and (5) a period of slow, continued reaction. C_3S remains fluid and workable during the dormant period [28] and the amount of free water remains relatively constant in the system [29]. All the rheological and water retention measurements were performed between 10 min and 1 h after the first addition of water (Fig. 2) (i.e., during the dormant period where changes in the rheological behavior can be ignored for the purpose of this paper).

2.2. Test of water demand

Water was gradually added to C_3S and at each step of water addition the same mixing procedure was applied. The water content required for the consistency to turn from that of a smooth paste into that of a cream is called the "point of water demand." It corresponds to the water content required to obtain the so-called normal consistency as determined according to ASTM C 187.

2.3. Filtration under gas pressure

Various pastes of C_3S corresponding to different initial water:solid ratios were filtered under an increasing pressure of nitrogen. The paste was poured into a 2-cm diameter filtration device from Millipore (Saint-Quentin-en-Yvelines, France). The average pore size of the filter was 0.45 μm. A small initial nitrogen pressure (5×10^{-3} Pa) was first applied 10 min after addition of water. The pressure was then gradually increased by increments of 5×10^{-3} Pa after equilibrium was established for each step of filtration. The corresponding volume fraction of solid ϕ_s for an applied pressure P is calculated with Eq. (14):

$$\phi_s = \frac{\text{volume solids}}{\text{volume solids + volume liquid}} = \frac{1}{1 + \frac{\rho_s}{\rho_w} \cdot \frac{w}{s}\left[1 - \frac{\Delta w}{w}\right]} \quad (14)$$

where Δw is the cumulative weight of water lost from 0 to P. Filtration was pursued until the point of gas percolation, which was detected by a pressure drop and by bubbles appearing in the filtrate. The consolidated cake was then ejected and weighed before and after drying. It should be noted that beyond the point of air entry, "volume solids + volume liquid" in Eq. (14) is not the total volume of the paste since part of it is occupied by air.

2.4. Rheology

The measurements were carried out with a computer-operated stress-controlled rheometer (AR 1000 from TA Instruments, Saint-Quentin-en-Yvelines, France) and were all done at 20°C. Pastes were prepared with w/s ranging from 0.70 to 0.43 (ϕ_s from 0.31 to 0.43). After mixing, the sample was loaded between two parallel plates 4 cm in diameter. The lower plate was rigid and enabled the measurement of the normal force applied on it. The upper plate (a scratched plate to prevent slipping) was lowered with the normal force closure option available with the rheometer and with a rotation speed of 2 s^{-1} (the gap was set at a value of 1.5 mm). Then a solvent trap was placed to prevent evaporation of water during the measurements. After 10 min of mixing, a preshear of 40 s^{-1} during 45 s and a rest period of 3 min were applied, and measurements started.

Two series of rheological measurements were performed on C_3S pastes: measurements in the so-called steady-state (or "static") shear mode, which give information on the flow behavior of the slurry, and measurements in the dynamic mode, which give information on the viscoelastic behavior. The steady-state mode destroys the structure that the slurry may exhibit at rest, whereas the dynamic mode preserves it, provided the stress or the strain does not exceed a critical value. The dynamic mode has been extensively applied to ceramic pastes, but not often to cement slurries [30–33].

A classical difficulty with steady-state shear measurements in pastes is obtaining a homogeneous strain within

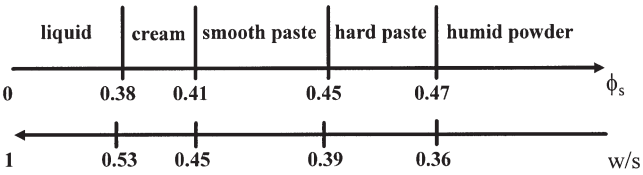

Fig. 3. Visual consistency of a C_3S and water mixture as a function of solid volume fraction ϕ_s (or w/s). "Humid powder" corresponds to a mixture with a rough, curdled surface aspect. "Hard paste" is a state where the surface is smooth but the rupture surfaces obtained by breaking a piece of paste still exhibit rough profiles. In a "smooth paste," these rupture surfaces are smooth. A "cream" cannot be broken, and when placed on a spatula, stays on it, whereas in the "liquid" state, the mixture spreads easily and pours out from the spatula. The passage from smooth paste into cream (here at $\phi_s = 0.41$) corresponds to the so-called point of water demand.

the paste layer. At very high concentration, the deformation tends to localize, either at the tool/paste interface (wall slip) or within the paste layer (rupture and internal slip). In our case, in spite of the scratched tool surfaces, we had difficulties performing reproducible steady-state measurements at solid volume fractions larger than 0.41.

In the dynamic mode, a sinusoidal stress is applied to the sample and the resulting sinusoidal strain is measured with a phase difference δ. For Hookean solids, stress and strain are in phase ($\delta = 0°$), and for Newtonian liquids, stress and strain are out of phase ($\delta = 90°$). For most materials, which are viscoelastic, δ is between 0 and 90°. The elastic and viscous components that contribute to the overall response are obtained by taking the ratio of the stress amplitude to the strain amplitude. This enables calculation of the complex modulus, G^*. The elastic (in phase) component is the storage modulus, G', while the viscous (out of phase) component is the loss modulus, G''. G' represents how well structured a material is and G'' represents viscous dissipation or loss of energy. All dynamic measurements were performed at an oscillatory frequency of 1 Hz.

3. Results

3.1. Water demand

Fig. 3 describes the evolution of the C_3S paste consistency as a function of concentration. The transition from a humid powder to a fluid occurs in a relatively narrow range of volume fraction of solid ranging from 0.47 to 0.37. The so-called point of water demand has been identified at $\phi_s = 0.41$, which is far below the random close-packing value for identical hard spheres (0.63) [15]. This indicates that the powder and the particles in the slurry contain agglomerates.

3.2. Pressure filtration

A series of filtrations on C_3S slurries with initial w/s ranging from 0.65 to 0.42 (initial volume fraction of solid ϕ_0 from 0.33 to 0.44) were performed. Fig. 4 shows ϕ_s plotted against applied pressure for the different slurries. The associated meniscus radii calculated with Eq. (12) are represented on the lower X-axis. The weight loss corresponding

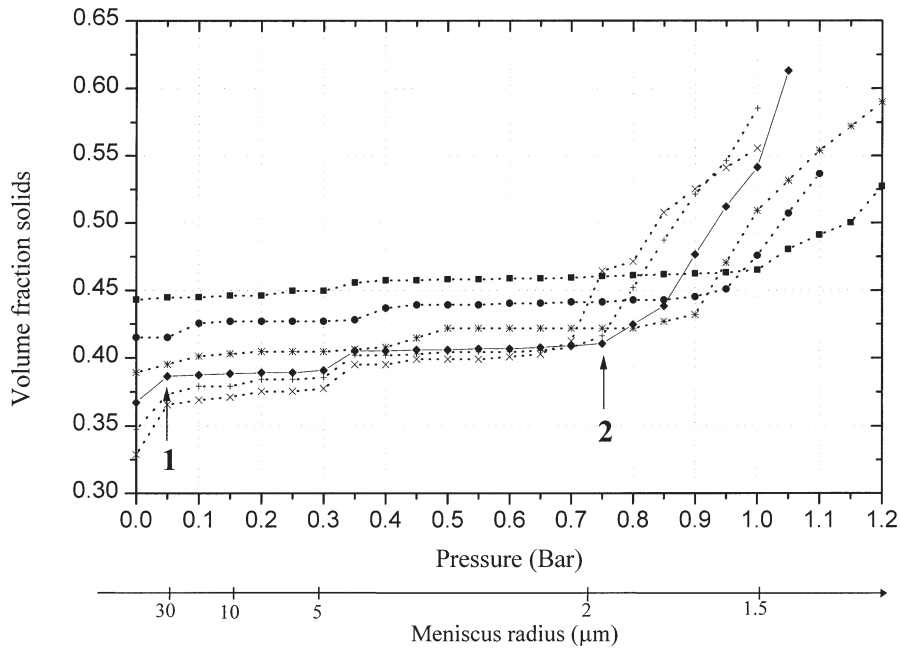

Fig. 4. Variation of the volume fraction of solids in C_3S slurries with initial w/s = 0.33 (×); 0.35 (+); 0.37 (◆); 0.39 (*); 0.41 (●); and 0.44 (■) as a function of pressure or corresponding meniscus radius (Young-Laplace Eq. 12). (1) First loss of weight at very low pressure (0.05 Bar) gives information on stability of the slurry, and (2) the point of air entry on floc structure. Meniscus radius before the point of air entry corresponds to interparticle distance and beyond to the structure pore size.

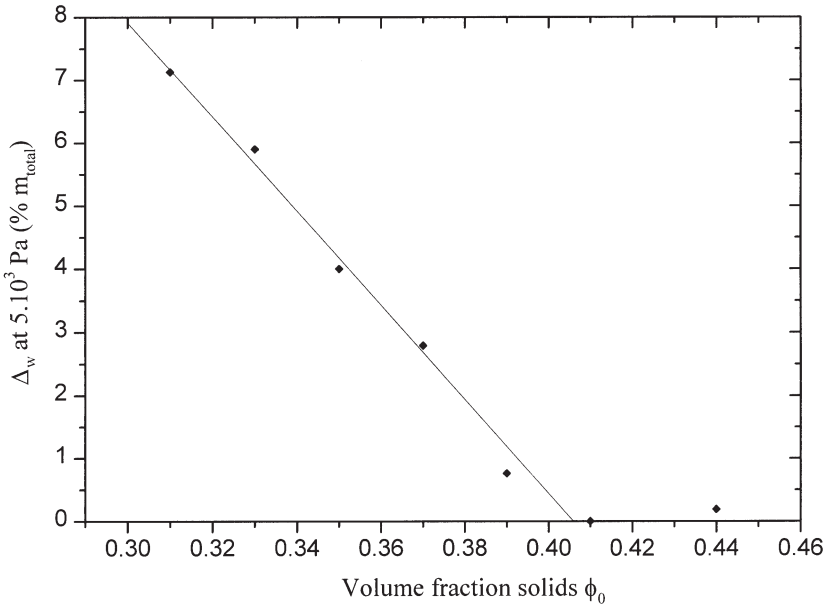

Fig. 5. Variation of initial loss of weight, Δ_w at 0.05 Bar, as a function of initial volume fraction of solids in the slurry, ϕ_0. When $\phi_0 > 0.39$ it becomes insignificant which illustrates the improvement of stability when fraction of solids increases.

to the first increase of ϕ_s, for $P = 5 \times 10^{-3}$ Pa ($r_k \cong 30$ μm), corresponds to the loss of quasi-free water from the slurry and therefore is an indicator of the degree of instability of the slurry. This loss of weight at low pressure decreases linearly with ϕ_0 (Fig. 5), indicating that stability is improved when ϕ_0 is increased. It vanishes at $\phi_0 = 0.41$.

At higher pressures, two regimes of water retention are observed (Fig. 4): a first regime where the volume fraction of solid varies slightly with pressure and that corresponds to the densification of the slurry to form a more rigid cake, and a second region where the pressure dependence is larger and that corresponds to the desaturation of the system. The point of gas entry is at the intersection between the two regimes. Both the pressure of gas entry P_{ae} and the corresponding volume fraction of solids ϕ_{ae} vary quasi-linearly with ϕ_0 (Fig. 6). The ϕ_{ae} values are related to the porosity of the cake structures. As illustrated in Fig. 6, the more diluted the initial slurry, the larger the porosity of the cake.

There is an upper limit of the solid volume fraction above which no water is lost before the pressure of air entry is reached. It corresponds to the boundary between saturated and nonsaturated systems and is about 0.47 in the present

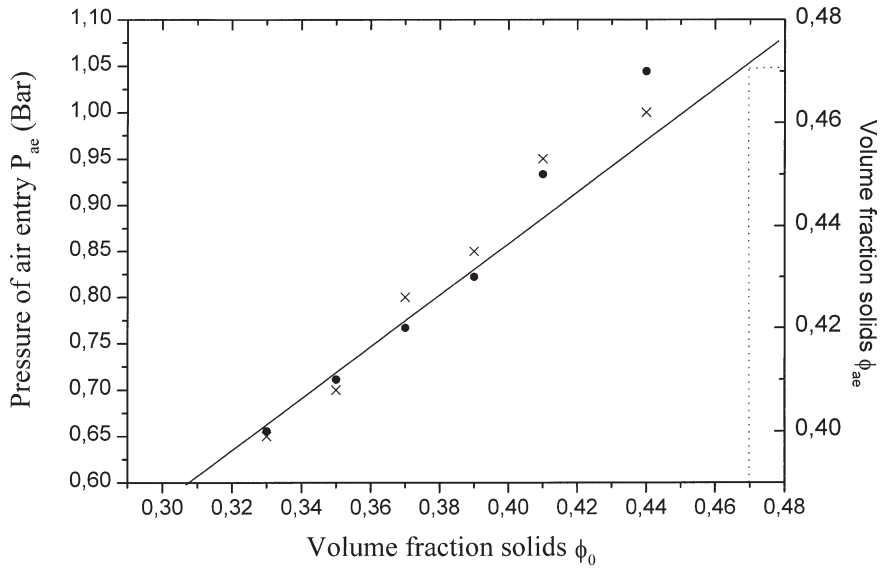

Fig. 6. Both pressure of air entry (×) and corresponding volume fraction of solids (●) vary linearly with initial volume fraction of solids of the slurry, ϕ_0.

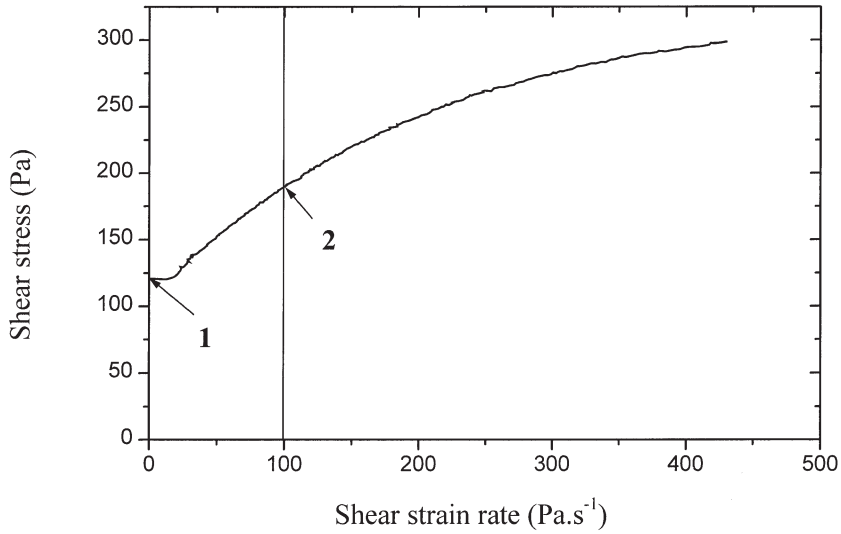

Fig. 7. Flow curve of a C_3S paste with w/s = 0.50. X-axis is the measured shear rate and Y-axis the applied shear stress. C_3S pastes exhibit plastic behaviour: the material does not begin to flow at zero stress but will once a critical stress (1) has been exceeded, and the subsequent behaviour is shear thinning. Then apparent viscosity has been calculated at a shear rate of 100 s^{-1} (2).

case. Interestingly, this corresponds to the transition from a humid powder to a hard paste as water is added in the water demand test (Fig. 3).

3.3. Rheology

3.3.1. Steady-state measurements

Flow curves describe the relationship between the shear stress and the shear rate on a sample. Fig. 7 represents a typical flow curve obtained with a slurry of C_3S with w/s = 0.50 (ϕ_s = 0.39). It exhibits clear plastic behaviour: the material does not begin to flow at zero stress but it does beyond a critical stress. Stress controlled rheometers allow raising the stress very smoothly from very low values before the sample starts flowing, and hence allow for the determination of the "true" yield stress directly (i.e., without requiring any extrapolation from the flow curve to zero shear rate). When the yield stress is exceeded, the shear rate increases suddenly and the sample exhibits shear thinning behavior (i.e., the viscosity decreases as shear rate increases). Classically this may reflect the breakdown of the structure in the system [34]. Instead of determining an extrapolated plastic viscosity value, we determined an apparent

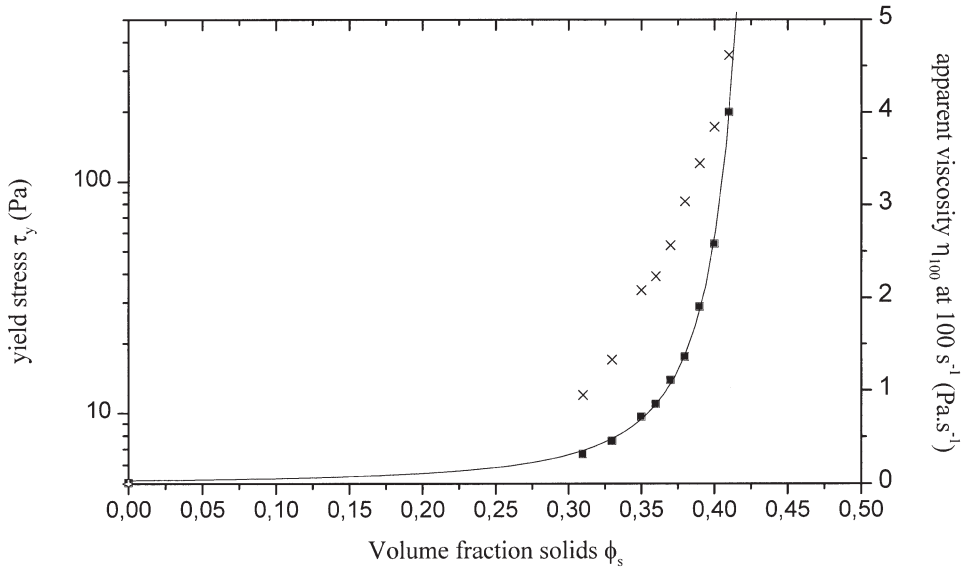

Fig. 8. True yield stress τ_y (×, log scale) and apparent viscosity η_{100} (■) at 100 s^{-1} plotted against volume fraction of solids for different mixes of C_3S and deionized water. Both τ_y and η_{100} increase when volume fraction of solids increases. Experimental apparent viscosities fit well the Krieger-Dougherty equation (continuous line).

viscosity as the derivative of stress vs. strain rate at some value of strain rate [35]. We arbitrarily chose a strain rate of 100 s^{-1}.

Fig. 8 displays the evolution of the yield stress and apparent viscosity as a function of the solid volume fraction. The viscosity data are well fitted by the Krieger-Dougherty equation in the range of solid volume fraction from 0.31 to 0.41. In the same range, the yield stress increases by a factor of 40. The fitting parameters values for Eq. (1) are η_c = 0.034, [η] = 4.48, ϕ_M =0.45, and the "goodness of fit" χ^2 = 0.002. The low value for ϕ_M confirms the strongly flocculated structure of the slurries. In highly concentrated slurries ($\phi_s \geq 0.41$) no reliable steady-state data could be obtained due to wall slip or fracture.

Regarding normal force measurements, concentrated slurries exhibit a sudden increase of the normal force when flow is initiated (Fig. 9). This behaviour is typical of dilatancy in granular media. Fig. 10 displays the amplitude of the normal force increase at the onset of flow for C_3S slurries as a function of volume fraction of solid. Three regions with different behaviours can be distinguished (Fig. 10): a first region for $\phi_s < 0.38$, where no variation of the normal force occurs; a second region up to $\phi_s = 0.41$, where dilatancy increases with ϕ_s; and a third region in the vicinity of the packing concentration, ϕ_M, where dilatancy still increases but with very large fluctuations in the data. The first regime is a normal, nondilatant, fluid regime, whereas the two other regimes give clear signs of a granular behavior. We will come back to this in the Discussion section.

3.3.2. Dynamic mode measurements

The variations in G' and G'' with strain for a C_3S slurry at $\phi_s = 0.39$ are displayed in Fig. 11. For a flocculated suspension, particles are able to elastically recover their microscopic position with respect to their neighbours as long as the strain, γ does not exceed some critical strain amplitude, γ_c. Below this critical strain amplitude, the material acts as an elastic solid. The flocculated network is preserved, and G^* is independent of strain. The material is in its linear viscoelastic regime (LVR). Above the critical strain, the network is destroyed and the modulus drops rapidly. For suspensions in general, the critical strain is not well defined in literature. Some authors consider that the material leaves the

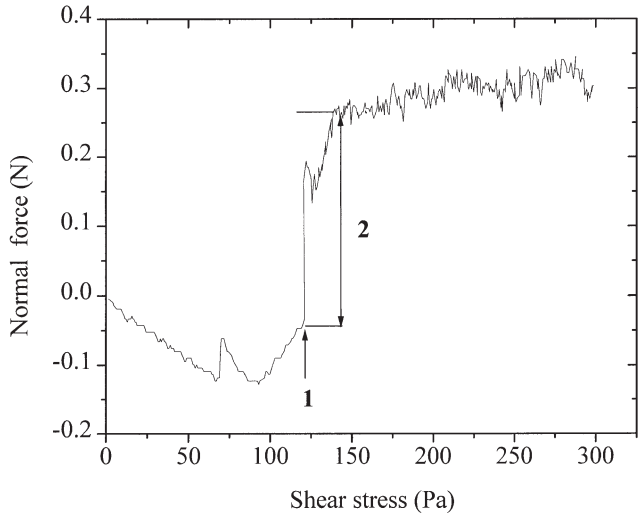

Fig. 9. Variation of the normal force applied on the lower plate during flow measurement (2) of a C_3S paste with w/s = 0.50 (ϕ_s = 0.39), when the yield stress (1) is exceeded.

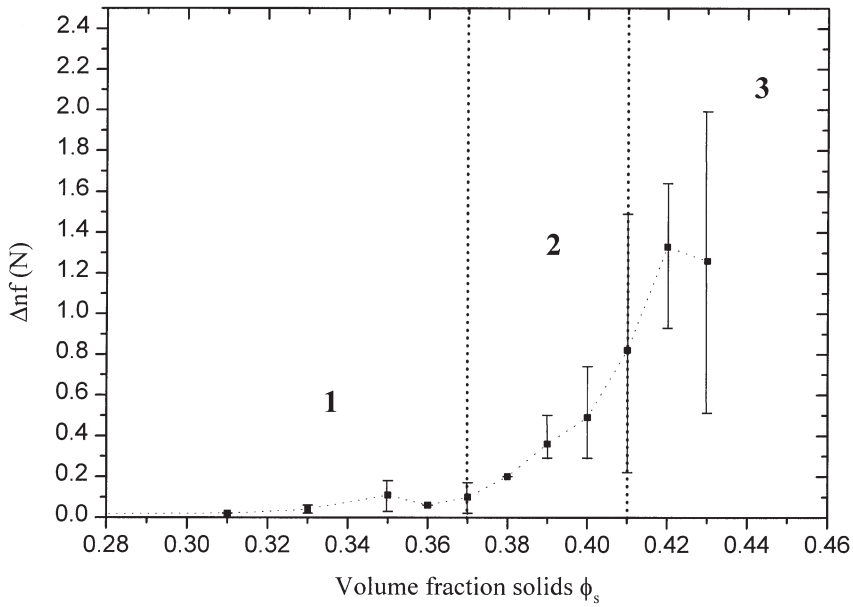

Fig. 10. Increase of normal force in C_3S pastes as a function of volume fraction of solids. The mean value of the normal force variation is represented with squares (■). Three behaviours are distinguishable: (1) a nondilatant behaviour, (2) a reproducible dilatant behaviour, and (3) a nonreproducible dilatant behaviour where normal force fluctuations are large.

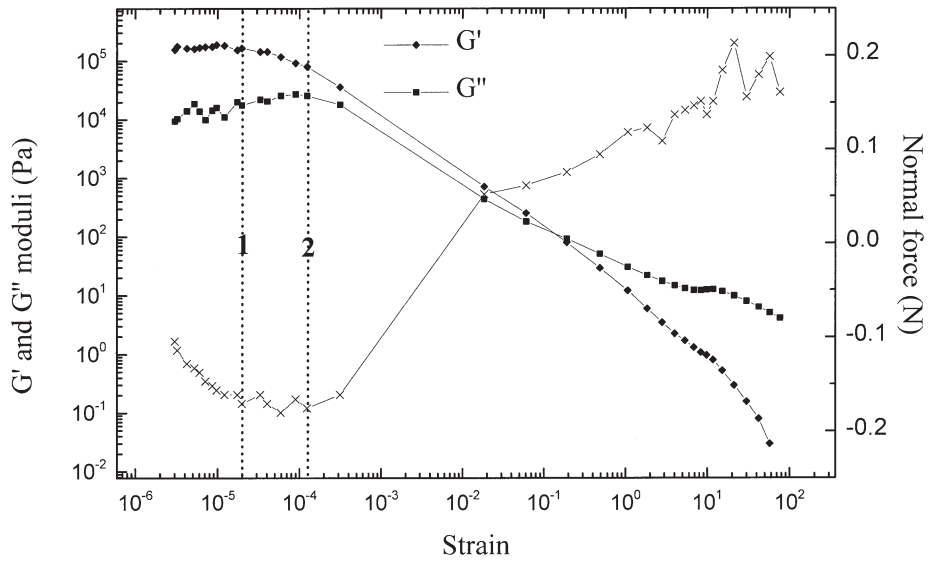

Fig. 11. Elastic (G') and loss (G'') moduli as a function of strain obtained with a torque sweep at 1 Hz for C_3S paste with $w/c = 0.50$ ($\phi_s = 0.39$). (1) is the strain where G' starts to decrease and (2) is the strain where G'' starts to decrease. Normal force measurements are represented with crosses (×).

LVR when G' begins to decrease [30], whereas others consider that both G' and G'' have to decrease [33]. In fact, the situation is slightly more complex since, as shown in Fig. 11, there is a range of strain where G' begins to decrease, reflecting the flocculated network rupture, whereas simultaneously G'' increases slightly (strain domain between marks 1 and 2 in Fig. 11). Such a behavior may be due to loss of energy by floc rupture and viscous dissipation by micro-flow disturbances [36]. The material does not act yet as a viscoelastic liquid because the network is not completely destroyed. Defining the limit of the LVR as the strain at which both G' and G'' start to decrease, we obtain 1.3×10^{-4}. This is in excellent agreement with the values obtained by other authors for fresh C_3S and cement pastes [30,33].

Another interesting (yet expected) point is the crossover between G' and G''. As long as the strain remains within the LVR, G' is larger than G'' by a factor of the order of 10, which is also in agreement with previous results on cement pastes and which is a clear sign of the essentially elastic behavior of the medium. As soon as the limit of the LVR is surpassed, the difference between G' and G'' starts to decrease and the crossover occurs at a strain of 10^{-1}. Beyond that point, G' becomes increasingly smaller than G'', reflecting the now essentially viscous nature of the medium.

As also shown in Fig. 11, the normal force measurements exhibit features corresponding remarkably well with the evolution of the moduli. The strain at which the normal force begins to increase is within experimental error the same as the strain where both G' and G'' start to decrease: about 2×10^{-4}. Thus, the onset of dilatancy, at least at this solid volume fraction, corresponds closely to the critical strain (according to the definition that we adopted). It corresponds also with the appearance of harmonics in the sinusoidal strain response.

The influence of the solid volume fraction on the dynamical rheological parameters is illustrated in Fig. 12, which displays the initial values of the complex modulus G^* for $\gamma \to 0$ and of the critical strain γ_c plotted as a function of ϕ_s. In the explored range of ϕ_s, γ_c remains quasi-constant at about 1.3×10^{-4}, except in the more diluted pastes where a (very) small increase is observed. For the modulus, there is a first domain, up to $\phi_s \cong 0.38$, where G^* varies but slightly with volume fraction of solid, and a second domain, beyond $\cong$ 0.38, where G^* increases strongly. This is also the solid volume fraction where a normal force increase starts to be detected. This will be discussed below.

4. Discussion and conclusion

Let us first discuss briefly two aspects of the steady-state and dynamic mode rheological measurements. First, our results confirm the previous observations [1] that the Krieger-Dougherty equation describes correctly the relationship between viscosity and concentration in cement pastes (Fig. 8). A surprising result, though, is that ϕ_M for C_3S pastes (0.45, this work) is much lower than for Portland cement, where it goes from 0.70 for well-dispersed (with superplasticizer) pastes to 0.64 for flocculated (without superplasticizer) pastes [1]. This suggests that flocculation is even higher (larger and/or more porous flocs) in the present case, increasing further the hydrodynamic volume of the solid fraction.

Second, our results confirm also that the critical strain of cementitious pastes is extremely small, of the order of 10^{-4}, whatever the w/c ratio (Fig. 12). Our C_3S pastes behave in this respect very much like Portland cement pastes [30], in

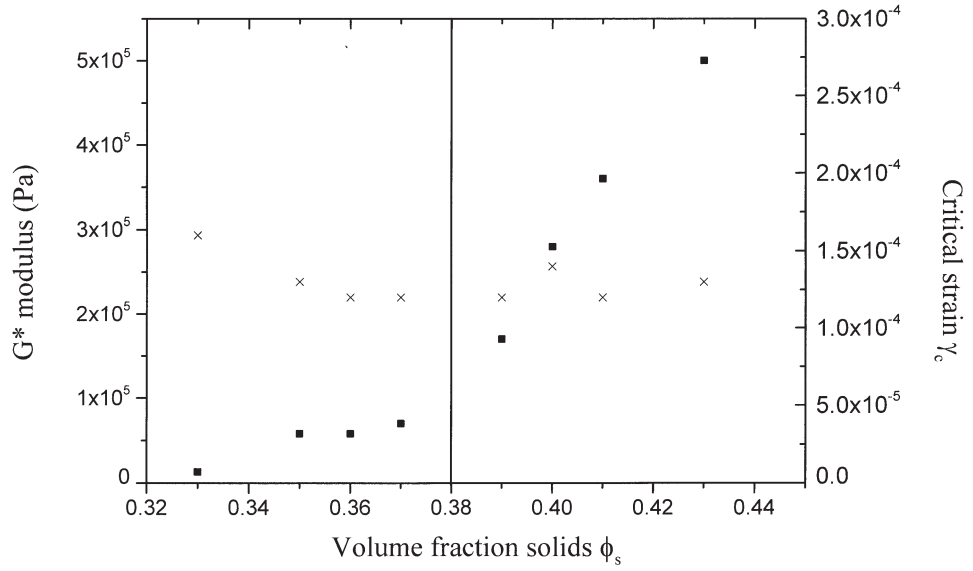

Fig. 12. Variations of the complex modulus, G^* (■), in the linear viscoelastic region and critical strain, γ_c (x), as a function of ϕ_s for C_3S slurries.

agreement with another recent study on C_3S [33]. As discussed by Goodwin [37], such small values are typical of coagulated suspensions where the particles form a continuous network held together by short-range surface forces, and that do not withstand large deformations without breaking or rearranging. Coagulation of the cement particle assemblies in fresh pastes has already been demonstrated by other techniques, such as ultrasonic dispersion [38]. It appears to be a general feature of cementitious pastes and has far-reaching consequences for the structural evolution of the medium since the coagulated network provides the framework within which all subsequent structural evolutions related to hydration will take place [38].

An illustration of this flocculation is the relationship between the initial solid volume fraction in the pastes and the pressure of air entry in the filtration experiments, although compaction has been achieved due to water departure. The smaller the initial solid fraction, the smaller the pressure of air entry (Fig. 6). In terms of pore size, via Eq. (12), this means that the smaller the initial solid fraction, the larger the size of the pores which are invaded by nitrogen when the packing becomes rigid (neglecting the contribution of shrinkage that arises from the development of capillary forces). In other words, the more diluted the starting paste, the more open the final rigid network. If the particles were well dispersed, such a "memory" effect would not be expected. One would rather expect a final state that would be independent of the initial concentration. Instead of this, there is a clear (though limited) memory of the initial state. In quantitative terms, the meniscus diameter obtained by applying the Laplace equation at the point of air entry is 4.3 μm ($P = 6.5 \times 10^4$ Pa) in the more diluted paste and 2.8 μm ($P = 10^5$ Pa) in the more concentrated. These values correspond to the maximum pore size within the filtration cake. For an ordered compact packing of spheres of diameter $d_0 = 8.5$ μm (the average C_3S particle diameter in the powder), the central hole within a tetrahedron of such spheres would be $0.225\ d_0 = 1.9$ μm. The first voids to be emptied by air when the filtration cake becomes rigid are significantly larger than that, as expected for a partially collapsed coagulated network.

The existence of a "memory" effect between the initial and compacted state of a cement paste has already been shown by Miller et al. [39] in compressive rheology experiments in which the paste was sedimented and compacted using a centrifuge. These authors measured the compressive yield stress, $P_y(\phi)$ (i.e., the load beyond which the bed consolidates irreversibly). A surprising result though was that $P_y(\phi)$ decreases as the initial volume fraction increases. The more diluted the starting paste, the larger the pressure range in which it responds elastically before consolidating irreversibly. This result was yet unexplained. It should be noted, however, that in the centrifuge technique the load is applied on the particles whereas in our gas filtration technique it is applied homogeneously on the paste as long as the particles are not in contact and on the liquid as soon as contact is reached and the packing becomes rigid.

Another interesting point is the evolution of the low pressure water loss in the filtration experiments (Figs. 4 and 5). It should be kept in mind that such a loss does not occur spontaneously under gravity but requires the application of a small stress ($\Delta P = 5 \times 10^{-3}$ Pa). This loss is nothing but the first step in the consolidation process of the paste leading finally, at the point of air entry, to a rigid porous structure. It is a qualitative indication of the stability of the paste. It may be seen that the low pressure water loss decreases considerably over a narrow range of initial solid volume

fraction, from a nonstable system at $\phi_0 = 0.31$ to a stable solid network at $\phi_0 = 0.41$. A quasi-rigid (i.e., uncompressible, network with no water loss up to air entry) is reached at $\phi_0 = \phi_{ae} \cong 0.47$ (Fig. 6).

We now turn to the comparative analysis of the three sets of results (water demand, gas pressure filtration, and rheology). When taken together, the data indicate the existence of two particular state boundaries:

1. $\phi_s = 0.38 \pm 0.05$. This is the liquidity limit, as defined in standard ASTM procedures. It is also the solid volume fraction value where the complex modulus in dynamic rheological measurements starts to increase. It is also the volume fraction where the normal force starts to be detectable (i.e., where dilatancy sets in). It should be noted that strictly speaking one should not detect a normal force because the lateral edges of the paste layer are free surfaces. The paste is hence free to expand laterally and, in an infinitely slow oscillatory shear, the volume expansion should occur in that direction without normal stress on the plates. Thus, the normal force that is detected is likely to be a dynamic and transient effect.
2. $\phi_s = 0.41 \pm 0.05$. This is the solid volume fraction value where the normal force fluctuations, typical of the contact statistics in granular media [15], begin to increase dramatically. It is also the value beyond which the initial weight loss in the filtration experiments is no longer observed. It is also the point where steady-state shear rheological measurements become difficult. Finally, it is the point of water demand, as defined in the ASTM standard procedure.

In addition, two other noticeable state boundaries are observed at higher concentrations: $\phi_s = 0.45$ corresponds to the point where the viscosity is expected to diverge according to the Krieger-Dougherty equation, and $\phi_s = 0.47$ is the concentration where in the filtration experiments there is no water loss at all before the point of air entry.

Based on the previous observations, a simple rheophysical scheme may be proposed in which the rheological behavior is related to the structure of the medium (Fig. 13). Three regimes may be defined:

- Below $\phi_s = 0.38$, the paste may be described as a suspension of flocs, containing excess water with respect to the void space of the flocs. The flocs do not yet form a continuous percolating (coagulated) network. The excess water, which is quasi-free water in thermodynamical terms, may be expelled by applying a very small pressure in a filtration experiment. At rest, bleeding may be expected. Under shear, the viscosity

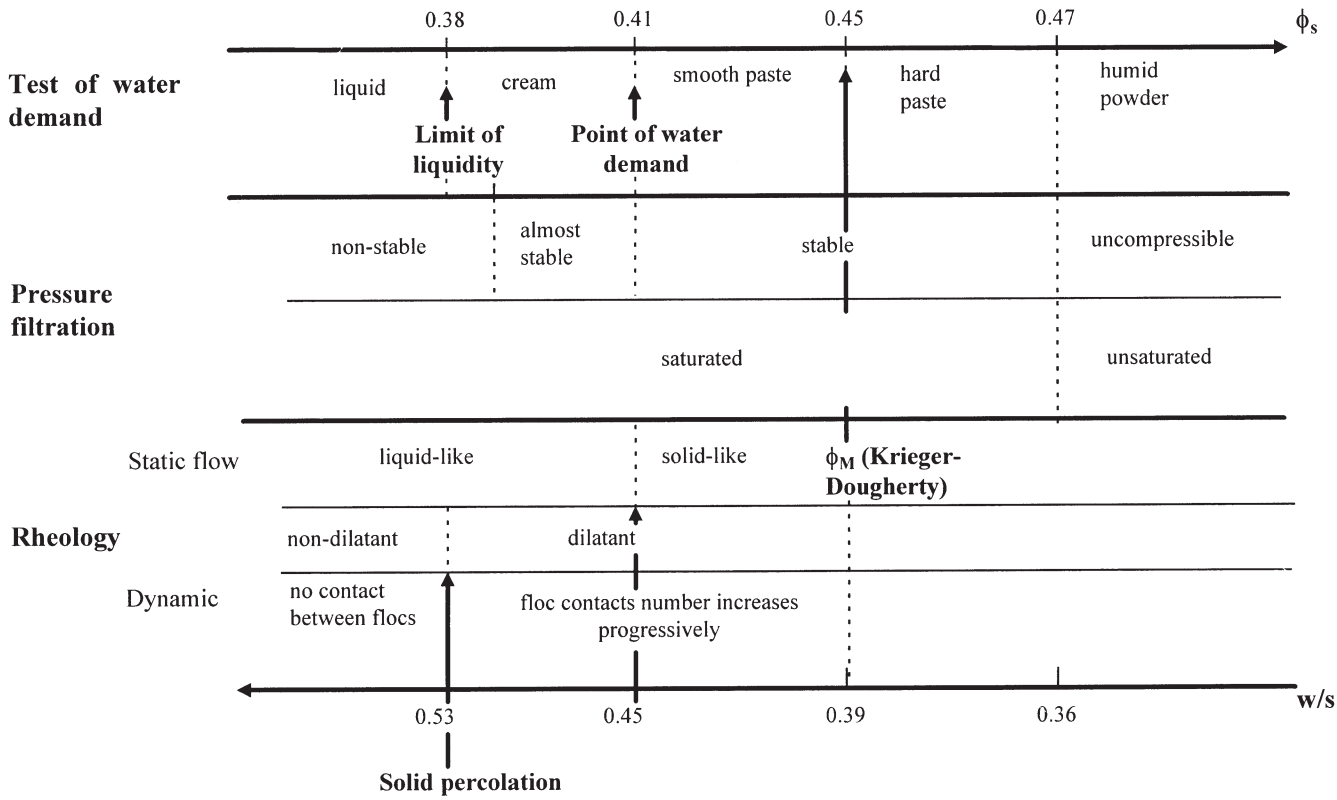

Fig. 13. Phase diagram of C_3S as a function of ϕ_s or w/s and its corresponding rheological behaviours. The liquid to solid transition occurs through an intermediate state where the material exhibits a dilatant granular-like behaviour between the limit of liquidity and the point of water demand. ϕ_M is the maximum volume fraction derived from Krieger-Dougherty equation.

follows Krieger-Dougherty equation, provided sedimentation can be avoided during the measurements.

- Above $\phi_s = 0.41$, the paste is best described at rest as a coagulated percolating network and, under shear, as a lubricated granular packing where the objects (flocs) are brought into contact. No excess, quasi-free, water is present, but the network is still significantly compressible in gas filtration experiments.
- For $0.38 \leqslant \phi_s \leqslant 0.41$, the system is in an intermediate regime where percolation develops as evidenced by the modulus increase. The amount of quasi-free water is gradually decreasing. The network may still be easily destroyed under shear and Krieger-Dougherty equation still applies. The occurrence of interparticle (flocs) contacts during flow is evidenced by the onset of dilatancy.

Further work on the modifications of this scheme in the presence of ions in solution and superplasticizers is in progress.

References

[1] L.J. Struble, G.K. Sun, Viscosity of Portland cement paste as a function of concentration, Advanced Cement Based Materials 2 (1995) 62–69.
[2] I.M. Krieger, T.J. Dougherty, Trans Soc Rheol 3 (1959) 137–152.
[3] I.M. Krieger, Adv Colloid Interface Sci 3 (1972) 111–136.
[4] M. Mooney, The viscosity of a concentrated suspension of spherical particles, J Colloid Sci 6 (1951) 162–170.
[5] R.C. Ball, P. Richmond, P Phys Chem Liq 9 (1980) 99–116.
[6] D. Quemada, Rheology of concentrated disperse systems and minimum energy dissipation principle—I. Viscosity-concentration relationship, Rheol Acta 16 (1977) 82–94.
[7] T. Nagatami, J Phys Soc Japan 47 (1979) 320–327.
[8] D. Bedeaux, Chem Phys Lett 94 (1983) 324–326.
[9] H.A. Barnes, J.F. Hutton, K. Walters, An Introduction to Rheology, Elsevier, New York, 1989, pp. 119–131.
[10] C.G. De Kruif, E.M.F. Van Iersel, A. Vrij, W.B. Russel, J Chem Phys 83 (1985) 4717–4725.
[11] D.A.R. Jones, B. Leary, D.V. Boger, J Colloid Interface Science 147 (1991) 479–495.
[12] C. Allain, M. Cloitre, B. Lacoste, I. Marsone, J Chem Phys 100 (1994) 4537–4542.
[13] O. Reynolds, Phil Mag 20 (1885) 468–481.
[14] R.A. Bagnold, Proc Roy Soc A 295 (1966) 219–232.
[15] H.M. Jaeger, S.R. Nagel, Science 255 (1992) 1523–1531.
[16] K. Kendall, In: B.J. Briscoe, M.J. Adams (Eds.), Tribology in Particulate Technology, Adam Hilger, Bristol, UK, 1987, pp. 91–102.
[17] K. Kendall, A.J. Howard, J.D. Birchall, Phil Trans Roy Soc A 310 (1983) 139–153.
[18] P. Dantu, Proc. 4th Int. Conf. Soil Mechanics and Food Eng., Vol. 1, London, 1957, p. 144.
[19] T. Wakabayashi, Proc. 9th Japanese National Congress on Applied Mechanics, Science Council of Japan, Tokyo, Japan, 1959, pp. 133–140.
[20] M. Ammi, T. Travers, J.P. Troadec, J Phys D 20 (1987) 424–431.
[21] G.W. Scherer, J Am Ceram Soc 73 (1990) 3–14.
[22] L.S. Richard, Soil Sci 51 (1941) 377–386.
[23] J. Persello, A. Magnin, J. Chang, J.M. Piau, B. Cabane, J Rheol 38 (1994) 1–26.
[24] G. Sposito, The Surface Chemistry of Soils, Oxford University Press, New York, 1984.
[25] A.W. Adamson, Physical Chemistry of Surfaces, John Wiley & Sons, Inc., New York, 1990.
[26] B.V. Velamakanni, F.F. Lange, J Am Ceram Soc 74 (1991) 166–172.
[27] H.F.W. Taylor, Cement Chemistry, Academic Press, New York, 1990.
[28] K.L. Scrivener, in: J. Skalny (Ed.), Materials Science of Concrete, American Ceramic Society, Westerville, OH, 1989, pp. 127–161.
[29] S.A. Fitzgerald, D.A. Neumann, J.J. Rush, D.P. Bentz, R.A. Livingston, Chem Mater 10 (1998) 397–402.
[30] M.A. Schultz, L.J. Struble, Use of oscillatory shear to study flow behavior of fresh cement, Cem Concr Res 23 (1993) 272–282.
[31] L.J. Struble, M.A. Schultz, Using creep and recovery to study flow behavior of fresh cement paste, Cem Concr Res 23 (1993) 1369–1379.
[32] L.J. Struble, W.G. Lei, Rheological changes associated with setting of cement paste, Advanced Cement Based Materials 2 (1995) 224–230.
[33] L. Nachbaur, A. Nonat, J.C. Mutin, L. Choplin, Dynamic mode rheology of cement pastes, 2d RILEM Workshop on Hydration and Setting, RILEM, Dijon, France, 1997.
[34] J. Mewis, A.J.B. Spaull, Adv Colloid Interface Science 6 (1976) 173–200.
[35] L.J. Struble, G.K. Sun, Cement viscosity as a function of concentration, Mat Res Soc Symp Proc 289 (1993) 173–178.
[36] P. Coussot, Mudflow Rheology and Dynamics, Balklema, Rotterdam, 1997.
[37] J.W. Goodwin, Rheology of ceramic materials, Am Ceram Soc Bull 69 (1990) 1694–1698.
[38] S.P. Jiang, A. Mutin, A. Nonat, Studies on mechanism and physicochemical parameters at the origin of the cement setting. I. The fundamental processes involved during the cement setting, Cem Concr Res 25 (1995) 779–786.
[39] K.T. Miller, W. Shi, L.J. Struble, C.F. Zukoski, Compressive yield stress of cement paste, Mat Res Soc Symp Proc 370 (1995) 285–291.